Doping Dependence of the Electronic Structure of $La_{1-x}Na_xMnO_3$ by Resonant X-ray Emission and X-ray Absorption Spectroscopy

F. Bondino,*,† M. Platé,†,‡ M. Zangrando,† M. Zacchigna,† D. Cocco,§ A. Comin,|| I. Alessandri,⊥ L. Malavasi,# and F. Parmigiani†,||

INFM-TASC, Beamline BACH, Basovizza-Trieste, Italy, Dipartimento di Fisica, Università di Pavia, Pavia, Italy, Sincrotrone Trieste, Area Science Park, Basovizza-Trieste, Italy, Dipartimento di Matematica e Fisica, Università Cattolica del Sacro Cuore, Brescia, Italy, Laboratorio di Strutturistica Chimica, Università degli Studi di Brescia, Brescia, Italy, Dipartimento di Chimica Fisica "M. Rolla" and INSTM, IENI/CNR unità di Pavia, Università di Pavia, Pavia, Italy

Received: October 24, 2003; In Final Form: January 29, 2004

The electronic structure of $La_{1-x}Na_xMnO_3$ ($x = 0$, 0.08, and 0.15) thin films is investigated by resonant X-ray emission spectroscopy (RXES) and X-ray absorption spectroscopy (XAS). The excitation energy of the Mn dd transitions is derived. For different carrier doping concentrations, a significant increase in the emission of the low-energy excitations is observed. This finding is consistent with the less-pronounced structural distortion and the increased density of empty e_g-like majority states in the lower part of the conduction band of the lightly doped samples.

I. Introduction

The doped manganese oxide compounds $Ln_{1-x}A_xMnO_3$ (Ln = lanthanoids; A = alkali or alkaline earth metals) are a class of complex materials exhibiting a rich phase diagram with an unusual variety of critical phenomena rarely observed in solid-state physics. In particular, the magnetic phase transitions occurring in conjunction with drastic changes in the resistivity and the recent observation in these compounds of a colossal magnetoresistance effect[1,2] have sparked a great number of investigations of these materials. This effort led to the discovery of new properties such as orbital and charge ordering and half-metallic character.[3,4]

These properties arise from the interplay among several competing structural and electronic mechanisms that are not fully understood, such as the cooperative Jahn−Teller distortions, double exchange, and magnetic microstructures. In particular, several issues need to be addressed, such as the interplay between occupied and unoccupied states as well as controversies concerning the strength of the electronic correlations and the role of phonons. It is therefore important to provide reliable experimental data to address the adequacy of current theoretical models to describe the observed phenomena.

A powerful technique to use in investigating the elementary excitations in solids with elemental specificity is resonant X-ray emission spectroscopy (RXES). In RXES, an incident X-ray photon excites a core electron to the absorption threshold, and the X-ray emission resulting from the decay of the excited state is energetically analyzed. In recent years, this spectroscopy has progressed remarkably, becoming an extremely effective tool to use in studying low-energy neutral electronic transitions, charge-transfer excitations, interband transitions, and energy-band dispersion.[5,6,7]

By strong analogy to resonant Auger spectroscopy,[8] two different behaviors can be identified in RXES. A resonant inelastic scattering (RIXS) or Raman-like process is established when the photon energy of the emitted radiation is related to the incoming photon energy, whereas a fluorescence-like regime is observed when the emission lines are detected at constant photon energy. Both regimes can be derived from the Kramers−Heisenberg equation describing the RXES process in a single-step model.[9]

In this paper, we report an experimental investigation of the electronic structure of lanthanum manganite thin films where La ions are partially substituted by Na ions. In particular, we report X-ray absorption spectroscopy (XAS) and RXES measurements across the Mn L_3 and O K thresholds of $LaMnO_3$, $La_{0.92}Na_{0.08}MnO_3$, and $La_{0.85}Na_{0.15}MnO_3$, highlighting the variations in the spectra with Na^+ doping.

For $x \leq 0.15$, $La_{1-x}Na_xMnO_3$, similarly to the divalent alkaline earth ion (Ca and Sr) substituted manganites, displays a transition from a ferromagnetic metallic to a paramagnetic insulating phase, accompanied by a colossal magneto-resistance (CMR) effect. In $La_{1-x}Na_xMnO_3$, the number of dopant ions needed to get the "optimally doped" phase is half that in the divalent alkaline earth ion manganese oxides. Furthermore, in these manganites the Jahn−Teller effect is less pronounced with respect to divalent alkaline earth ion substituted systems with the same hole concentration because the tolerance factor[10,11] is close to 1.[12,13]

The novelty of this work is the observation of significant variations of the low-energy electronic excitations for different carrier doping concentrations. We explain these effects by considering the weaker hybridization of the t_{2g} and O 2p electrons due to a less-pronounced structural distortion in the substituted samples and to the higher density of empty e_g majority states in the lower part of the conduction band.

* Corresponding author. E-mail: bondino@tasc.infm.it.
† INFM-TASC.
‡ Dipartimento di Fisica, Università di Pavia.
§ Sincrotrone Trieste.
|| Università Cattolica del Sacro Cuore.
⊥ Università degli Studi di Brescia.
Dipartimento di Chimica Fisica "M. Rolla" and INSTM, Università di Pavia.

10.1021/jp037224z CCC: $27.50
Published on Web 03/05/2004

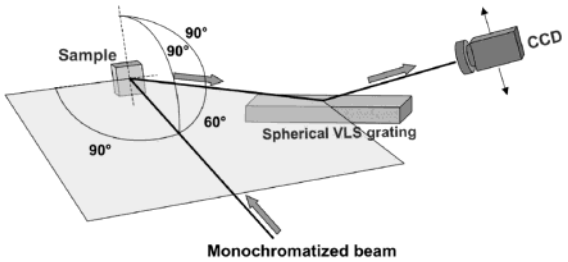

Figure 1. Experimental setup and scattering geometry for the RXES measurements at the BACH beamline.

II. Experimental Section

The data were obtained at the Beamline for Advanced diCHroism (BACH)[14,15] on the 8.1 helical undulator of the Elettra accumulation ring. Resonant emission spectra were acquired with the ComIXS fluorescence spectrometer.[16] The spectrometer is equipped with two variable-line-spacing spherical gratings with central groove densities of 4800 l/mm (optimized for the 20−200-eV region) and 19 200 l/mm (optimized for 150−1200 eV) and a 20 × 20 μm^2 pixel CCD detector.[17] The small spot size of the radiation on the sample (15 × 250 μm^2) allows the use of an entrance slitless design and the collection of a solid angle of about 30 × 10 $mrad^2$.

The first set of Mn L_3 emission spectra were recorded in fourth-order diffraction with the 4800 l/mm grating. The energy bandwidth of the incident photon beam for RXES was set at 0.7 eV at the Mn L_3 threshold, which corresponds to high flux and a resolving power of ∼930. During a second beamtime, Mn L_3 and O Kα emission spectra were recorded in second-order diffraction with the 19 200 l/mm grating. In the Mn L_3 line in second-order diffraction (emission energy ∼320 eV), the number of counts on the elastic peak was about 300/min for a 230-mA ring current and with the slits set to 30 μm. The elastic-peak fwhm at the Mn L_3 threshold was 1.1 eV. Under the same conditions, 7600 counts/min were detected on the elastic peak in the O Kα line in second-order diffraction (emission energy ∼265 eV).

XAS spectra were obtained in total-electron-yield mode, measuring the sample drain current with a photon resolution of 0.28 eV. The incident photon energies were calibrated using the elastic peak measured in the X-ray emission spectra.

The scattering geometry and the experimental setup for the RXES measurements are shown in Figure 1. The spectra were collected both with vertical polarization (i.e., the electric vector of the incident radiation perpendicular to the scattering plane highlighted in Figure 1) and horizontal polarization (i.e., the electric vector in the scattering plane).

The samples were 150-nm thin films of $La_{1-x}Na_xMnO_3$ ($x = 0$, 0.08, and 0.15) grown ex situ on polycrystalline Al_3O_2 by radio-frequency magnetron sputtering. $LaMnO_3$ was obtained from La_2O_3 and Mn_2O_3, and $La_{1-x}Na_xMnO_3$ samples were prepared by adding Na_2CO_3 to the lanthanum and manganese oxides. Details of the sample preparation and its magnetic and electrical characteristics are reported elsewhere.[12] The transition temperatures, T_c's, from the ferromagnetic metallic phase to the paramagnetic insulating phase were ∼250 and ∼200 K for the $x = 0.15$ and 0.08 samples, respectively.[18] In these compounds, the lattice distortion decreases with Na substitution.[19]

III. Results

The Mn $L_{3,2}$ XAS spectra of $LaMnO_3$, $La_{0.92}Na_{0.08}MnO_3$, and $La_{0.85}Na_{0.15}MnO_3$ samples measured at 300 K with linearly polarized radiation are shown in Figure 2. The L_3 region of the spectra is clearly dependent on the composition. In $La_{0.85}Na_{0.15}MnO_3$, three features can be identified. A leading peak at 647 eV (I), a weak peak at about 645 eV (III), and another small structure (II) between these two peaks can be observed in the XAS spectra in Figure 2. In $La_{0.92}Na_{0.08}MnO_3$, peak III is less intense. In $LaMnO_3$, peak III is very weak, and structure II is more pronounced. No significant differences are observed between the Mn L_{23} XAS spectra recorded at 300 K (above T_c) and at 150 K (below T_c).

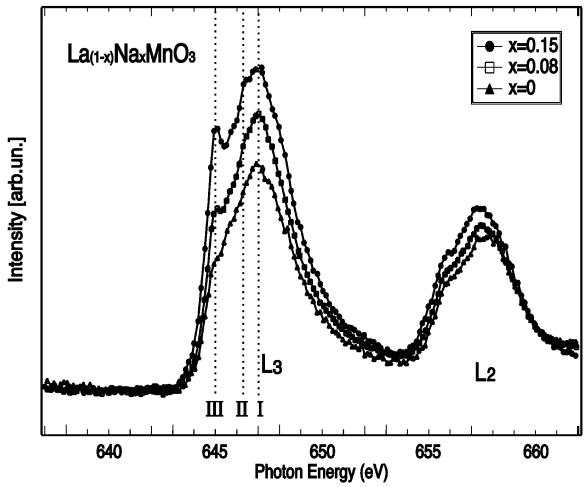

Figure 2. Doping-dependent Mn $L_{3,2}$ XAS for $La_{1-x}Na_xMnO_3$ ($x = 0$, 0.08, and 0.15).

Figure 3b shows the Mn $L_{3,2}$ (3d, 4s → 2p) RXES spectra obtained with vertically polarized radiation from the $x = 0.08$ sample at 300 K. In this configuration, the peak at zero energy loss (i.e., the elastic peak) is visible in almost all of the spectra, allowing an accurate calibration of the energy scale. The RXES data are plotted versus an energy-loss scale relative to the elastic peaks. The excitation energies are indicated with ticks in the XAS spectrum shown in Figure 3a.

The RIXS and fluorescence-like features can be easily identified. The fluorescence-like features appear at constant emission energy (hence, as dispersing peaks in the figure). The RIXS features appear at constant energy, below the elastic peak. Two well-resolved RIXS structures are observed between excitation energies of 644 and 647 eV. A broad structure A at about 6−9 eV and another broad emission B at about 2−4 eV below the elastic peak can be observed in the RXES spectra in Figure 3b. The energy position of these RIXS losses is similar to those found in the Mn L_3 emission spectra of the related manganites compounds such as $Eu_{1-x}Ca_xMnO_3$ and $Pr_{0.5}Sr_{0.5}MnO_3$.[20,21]

The same RXES spectra were also recorded with horizontal polarization (i.e., with the electric vector of the incident light in the scattering plane). In Figure 3b, one of these spectra is displayed as a dotted line at $h\nu = 647$ eV. In this scattering geometry, the elastic peak is strongly suppressed, and inelastic features can be resolved more easily. Figure 3c shows the doping-induced changes in the electronic structure of $La_{1-x}Na_xMnO_3$. The spectra are displayed on an emission energy scale.

For the sake of comparison, the spectra have been normalized to the photon flux and the acquisition time. After this normalization, the intensity of the elastic peak for the undoped sample is always weaker than that for the doped-samples case. To follow the evolution of the inelastic features, we have arbitrarily further normalized the spectra to the intensity of the elastic peak. After performing this normalization, we find that the intensity of the O K_α NXE peaks, recorded simultaneously to the Mn L_3 RXES

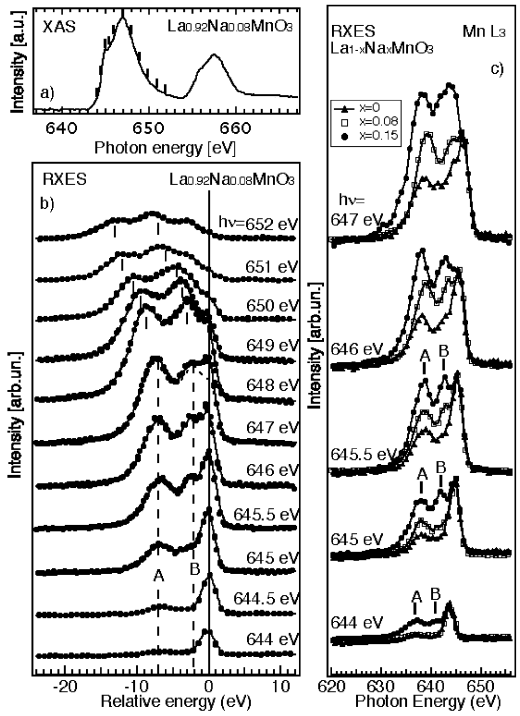

Figure 3. (a) Mn $L_{3,2}$ XAS of $La_{0.92}Na_{0.08}MnO_3$ at 300 K. (b) RXES spectra measured for fourth-order diffraction with the 4800 l/mm grating and vertically polarized radiation from the same $La_{0.92}Na_{0.08}MnO_3$ sample at different excitation energies across the Mn L_3 threshold at 300 K. One of the spectra recorded with horizontal polarization is shown (black dotted line, at 647 eV excitation energy). The RXES data are plotted against the transferred energy (curves are offset for clarity), and the excitation energies are indicated with ticks in the XAS spectrum. (c) Variation of the Mn 3d → 2p RXES spectra of $La_{1-x}Na_xMnO_3$ with Na concentration ($x = 0$, 0.08, and 0.15). The spectra are displayed in the emission energy scale, and data are normalized to the elastic emission peak.

spectra, turns out to be nearly constant for the different doping concentration, whereas the intensity of emission B increases with Na concentration. Independent of the normalization procedure at low excitation energies, such as 644 and 645 eV, peak B was absent in the $x = 0$ sample but it was present in the $x = 0.15$ sample.

A set of higher-resolution Mn L_3 spectra were obtained by using the 19 200 l/mm grating. Figure 4 shows these spectra together with a possible decomposition of the individual spectral structures after Gaussian fitting with six components. The spectra are plotted against the transferred energy, and the data are normalized to the photon flux. The component on the far right is E and refers to the elastic peak. Four inelastic peaks are also identified at −2.1, −3.3, −7.0, and −9.8 eV and are labeled with the letters B2, B1, A2, and A1, respectively. Finally, peak D, at constant emission energy, is detected at 635.4 eV.

At 650.2 eV, the spectrum apparently seems to be dominated by normal fluorescence.

In the O K XAS spectrum of $La_{0.85}Na_{0.15}MnO_3$ recorded at room temperature, a prepeak centered at 533.2 eV, a central structure that peaked at 540 eV, and a third structure at 546 eV are observed.

The O Kα (2p → 1s) RXES spectra were measured at several excitation energies across both the prepeak and the main absorption edge.

The weak elastic peak in the O Kα RXES spectra was enhanced by recording the O Kα emission spectra with vertical

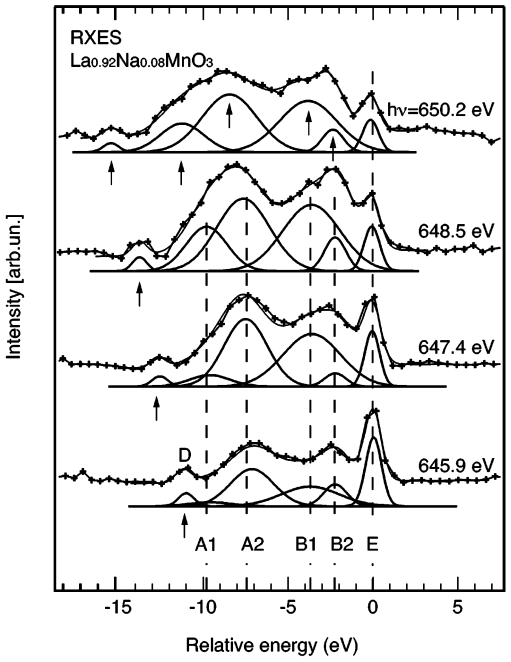

Figure 4. Gaussian fit of the inelastic peaks of a RXES spectrum of $La_{0.92}Na_{0.08}MnO_3$ at 300 K measured for second-order diffraction with the 19 200 l/mm grating at several incident photon energies. The spectra are plotted against the transferred energy, and the data are normalized to the photon flux. Emission A is deconvoluted into two components A1 and A2. Emission B is deconvoluted into B1 and B2.

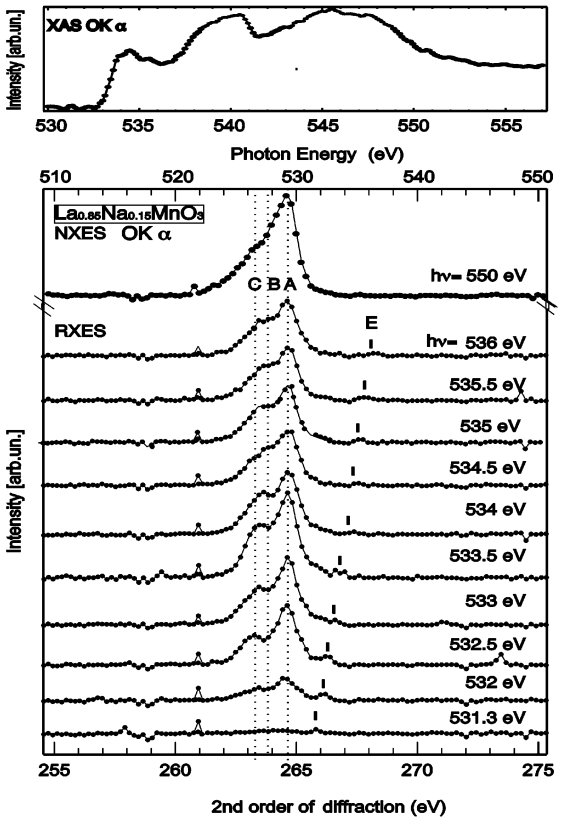

Figure 5. (Top) O K XAS of $La_{0.85}Na_{0.15}MnO_3$ at 300 K. (Bottom) Set of O 1s RXES spectra measured for second-order diffraction with the 19 200 l/mm grating with vertical polarization from the same $La_{0.85}Na_{0.15}MnO_3$ sample at 300 K.

linear polarization of the incident light. Figure 5 displays a set of O Kα RXES spectra obtained for $x = 0.15$ at 300 K. A clear dependence as a function of the incident photon energy can be

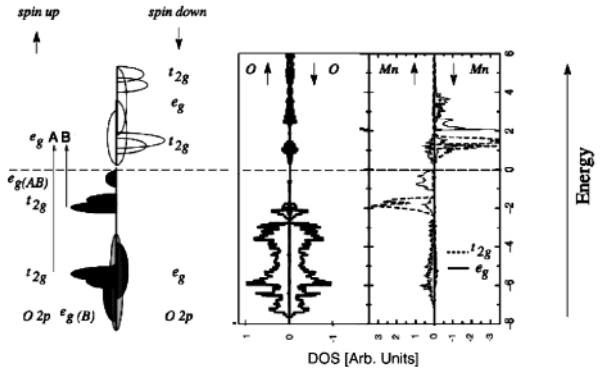

Figure 6. Mn 3d and O 2p partial DOSs for $LaMnO_3$ with the orthorhombic $GdFeO_3$ structure obtained by full-potential linearized augmented plane-wave LSDA calculations. Adapted from ref 23.

observed. When the excitation energy is tuned to the preedge peak, the emission spectrum of $La_{1-x}Na_xMnO_3$ exhibits a double-peak shape, whereas it is narrower on the main absorption structure. At excitation energies well above the O K absorption threshold, the peak again becomes strongly asymmetric, with the main peak having some spectral weight on the lower-photon-energy side. No Raman-like features are visible, but several emission lines at constant energy, whose intensity changes with the incident photon energy, are detected.

Elastic peak E is visible in several spectra, allowing a calibration of the energy scale. Besides elastic peak E, an intense emission (A) at 529.2 eV is observed at all energies, starting from 531.3 eV. In the prepeak region, starting from 532 eV, a second peak C at 526.9 eV is clearly visible. Above 533.5 eV, this component starts to decrease, and a new peak B at 527.3 eV can be resolved. At excitation energies well above the threshold, emission A presents a broad shoulder toward the lower photon energy.

In the prepeak region of the OK XAS and well above the threshold, the RXES spectra of the three samples are very similar, whereas in the 540- and 546-eV regions an intense spectral structure at 524.6 eV is detected in the RXES spectra of the undoped sample. The same feature is also detected in the doped samples, but it is much weaker.

IV. Discussion

The doping dependence of the Mn $L_{3,2}$ XAS spectra of the $La_{1-x}Na_xMnO_3$ compounds is similar to that observed in divalent alkaline earth ion substituted manganites.[22] In particular, the spectra display a change in shape consistent with a variation of the ground state from almost pure ^5E_g ($3d^4$) character to a mixture of ^5E_g and $^4A_{2g}$ ($3d^3$) (considering the octahedral symmetry of the Mn sites).[22]

The main features in the resonant Mn L_3 emission spectra can be identified and labeled according to an energy-level diagram based on spin-polarized density functional theory (SP-DFT) such as that found in refs 23 and 24. In absence of electronic structure calculations for $La_{1-x}Na_xMnO_3$ compounds, the partial DOS of $LaMnO_3$ was used as a starting point for the discussion. In Figure 6, the results of recent ab initio partial DOS calculations for distorted orthorhombic $LaMnO_3$ and the schematic diagram of the observed transitions are shown.[24]

According to these calculations, Mn e_g-like majority bands split by a strong electron−phonon coupling of the Jahn−Teller type give the dominant contribution to the density of states (DOS) closer to E_F. Calculations show that both the Mn t_{2g} and e_g σ bonding bands, hybridized with O 2p states, give a broad contribution to the occupied DOS around 5−6 eV. Peak A in Figure 3b and c can be assigned to an electronic excitation from this band to the empty e_g σ band.

Theory further shows that Mn t_{2g} electrons are well localized at −2 eV. Emission B (Figure 3b and c) is attributed to dd transitions from the occupied t_{2g} electrons to the e_g-like majority empty states.

Finally, structure D in Figure 4 can be identified as a normal fluorescence peak for the constant energy position of this peak.

The intensity of emission B increases significantly by increasing the Na^+ concentration. This effect can be qualitatively explained by considering the weaker hybridization of the t_{2g} and O 2p electrons due to a less-pronounced structural distortion in the substituted samples. The strong enhancement of peak B in the doped samples can also be explained by the higher density of empty e_g majority states in the lower part of the CB related to the presence of the Mn^{4+} ions. Also, emission A shows a similar dependence on the Na concentration, which can also be explained by the decrease of t_{2g} O admixing and the gradual depletion of the Mn e_g majority band with increasing *x*. However, the ratio between the intensity of A and B emissions does not show a clear trend either as a function of Na concentration or as a function of the excitation energy. Additional transition channels contributing to the intensity of emission A and the different energy-dependent cross sections for the two processes in the resonance regime can explain this behavior.

It is meaningful to compare the Mn L_3 RXE data with optical conductivity measurements because they also probe elementary excitations, though without elemental selectivity and different selection rules. In contrast to optical dipole transitions, RIXS emission can be described on the basis of monopole or quadrupole transitions, hence dd transitions are allowed.

The optical absorption spectra of alkali-doped and undoped $LaMnO_3$ display, below 10 eV, several broad bands near 1.3−1.8, 2−3, 5, 7, and 8−9 eV.[25,26] Most of these features, with the exception of those at 1.3 and 5 eV, are also detected in the RXE spectra. The lowest-energy transition below 2 eV is not resolved in the RXES data probably because it is hidden below the elastic peak, which is unusually broad. Its width (in second-order diffraction) is 1.1 eV, although the theoretical value is around 0.4 eV. The absence of the 5-eV transition in the Mn L_3 RXES spectra supports the assignment of this optical structure to a transition originating from O 2p states. The other bands should involve Mn 3d states because they are resonantly enhanced at the Mn L_3 threshold.

This interpretation is supported by the comparison of the RXES data with Mn L_3 resonant photoemission valence-band spectra (RPES) measured on the related $La_{1-x}Ca_xMnO_3$ manganites.[27] Because, according to calculations,[23] the e_g-like majority empty states are distributed close to the Fermi level and RXES is governed by spin selection rules, the Mn L_3 inelastic-scattering peaks in manganites can be associated with structural features in the valence band. In this way, a more detailed assignment of the spectral structures obtained from the Gaussian fitting of the Mn L_3 RXES data can be made. The RPES spectra were decomposed using seven Gaussian-like features centered at 1.7, 2.9, 4.1, 5.8, 7.8, 9.6, and 11.1 eV. The 2.9- and 4.1-eV emissions, assigned to Mn 3d states with t_{2g} and e_g ($3z^2-r^2$) symmetry, respectively, can be identified with the B2 (−2.1 eV) and B1 (−3.3 eV) RXES spectral components derived from the fitting deconvolution (Figure 4), although the 7.8- and 9.6-eV features, assigned to Mn 3d−O 2p π and σ bonds, match well with the A2 (−7.0 eV) and A1 (−9.8 eV) structures in the RXES spectra (Figure 4). As clear

from Figures 3 and 4, the 650.2-eV peak is already dominated by normal fluorescence emission and the inelastic structures are located at constant emission energies with A1 and A2 peaks starting to show normal fluorescence behavior at slightly lower excitation energies than B1 and B2 peaks.

The O K XAS is associated with the O 1s → 2p dipole transition. Because of the itinerant character of the O 2p states and the strong hybridization of the O 2p orbitals with the unoccupied Mn 3d/4s, La 5d/4f, and Na 3s orbitals, O K XAS spectra reflect the unoccupied conduction band.[28] The O K XAS spectra of the 0.08 and 0.15 samples look very similar to the corresponding spectra of the relative Sr- and Ca-doped manganites.[22,29] The absorption prepeak in manganites is attributed to the covalent mixing of the O 2p−Mn 3d unoccupied states. The feature centered at ∼540 eV consists of La 5d−O 2p hybridized states, and the structure centered at 546 eV originates from Mn 4sp−O 2p hybridization.

The O Kα RXES spectra of the $La_{1-x}Na_xMnO_3$ manganites displays a strong excitation-energy dependence similar to that observed in several perovskite copper oxides.[30,31] However, in the O Kα RXES spectra of related $Pr_{1-x}Sr_xMnO_3$ and $Eu_{1-x}Ca_xMnO_3$ manganites, no excitation-energy dependence in O Kα emission was observed.[20,21,32]

According to Anderson impurity-model calculations,[9] a strong dependence of the O Kα RXES line shape on the incident X-ray energy in hole-doped systems can be due to the different contribution by inequivalent oxygen ions in the manganite structure (i.e., in-plane and apical oxygen sites).

Considering the result of energy-band calculations for distorted orthorhombic $LaMnO_3$ (Figure 5 in ref 23), we find that the experimental RXES spectral structures well match the overall shape of the calculated O 2p DOS. Dominant peak A in O Kα RXES spectra can be attributed to the O 2p valence band ∼3 eV below the Fermi level.

For excitation energy tuned across the O K absorption preedge, the relative intensities of structures B and C detected in the high-photon-energy tail depend strongly on the photon energy. We thus suggest that structures B and C can be due to in-plane and apical O 2p states between 5 and 7.5 eV. According to the calculations, these states are more strongly hybridized to the Mn 3d valence band; furthermore, in this energy region the largest differences between in-plane and apical states are observed. From a heuristic comparison of the experimental spectra to the site-projected DOS from ref 23, we can argue that at low excitation energies (e.g., 532.5 eV) the double-peaked shape of the inelastic emission structure is associated with the selective excitation of a single O site. At higher energies (e.g., 534.5 eV), at least three structures can be identified, and we can argue that both oxygen sites are contributing to the emission spectrum. However, this qualitative consideration needs to be verified by specific calculations. Even in the absence of these specific calculations for the Na-substituted samples, the photon-energy dependence of O Kα RXES spectra of the doped samples can be also associated with the site-selective variation of the absorption cross section from inequivalent ions at different excitation energies.

V. Conclusions

In this paper, we reported RXES and XAS measurements across the Mn $L_{2,3}$ and O K thresholds of $La_{1-x}Na_xMnO_3$ (x = 0, 0.08, and 0.15) thin films. In particular, we have studied the influence of different Na concentrations on the valence and conduction bands by considering the effect of Mn 3d−O 2p hybridization as well as the structural distortion of the Mn−O bonds. The resulting information about the low-lying excitations is crucial because the intriguing interplay between the transport and magnetic properties of these materials, such as the CMR, is strongly correlated to the electronic configuration near the Fermi level.

In the RXES spectra, two broad RIXS structures at 2−4 and 6−9 eV and another fluorescence-like feature were detected. RXES data were compared with optical conductivity measurements, valence photoemission data, and SP-DFT partial DOS calculations for $LaMnO_3$. The model used to interpret the RIXS emissions, in the undoped sample, is in good agreement with experimental data on the elemental-selective bulk electronic structure. The result provides support for the reliability of recent band-structure calculations. In light of this, the RIXS data for the Na-substituted materials, whose electronic structure is unknown, have been interpreted in the framework of the available models.

The intensity of the RIXS structures displayed a significant increase with doping. This effect was related to the systematic decrease of the lattice distortion and the gradual increase of the e_g-like majority empty states by increasing the Na concentration. A significant dependence on the excitation energy was also observed in the O Kα RXES spectra of these compounds and was attributed to the site-selective variation of the absorption cross section from in-plane and apical oxygen sites at different excitation energies.

Acknowledgment. This work was supported by the INFM LdS-BACH project. We gratefully thank K.C. Prince, M. Matteucci, M. Finazzi, and G. Zampieri for useful suggestions and fruitful discussions.

References and Notes

(1) von Helmolt, R.; Wecker, J.; Holzapfel, B.; Schultz, L.; Samwer, K. *Phys. Rev. Lett.* **1993**, *71*, 2331.

(2) Jin, S.; Teifel, T. H.; McCormack, M.; Fastnacht, R. A.; Ramesh, R.; Chen, L. H. *Science* **1994**, *264*, 413.

(3) Coey, J. M. D.; Viret, M.; von Molnar, S. *Adv. Phys.* **1999**, *48*, 167.

(4) Dagotto, E. *Nanoscale Phase Separation and Colossal Magnetoresistance: The Physics of Manganites and Related Compounds*; Springer Series in Solid-State Sciences; Springer-Verlag: Berlin, 2003; Vol. 136.

(5) Special issue of *J. Elect. Spectrosc. Relat. Phenom.* **2000**, *110−111*.

(6) Butorin, S. M.; Guo, J.-H.; Magnuson, M.; Nordgren, J. *Phys. Rev. B* **1997**, *55*, 4242.

(7) Kuiper, P.; Guo, J.-H.; Såthe, C.; Duda, L.-C.; Nordgren, J.; Pothuizen, J. J. M.; de Groot, F. M. F.; Sawatzky, G. A. *Phys. Rev. Lett.* **1998**, *80*, 5204.

(8) Finazzi, M.; Ghiringhelli, G.; Tjernberg, O.; Ohresser, Ph.; Brookes, N. B. *Phys. Rev. B* **2000**, *61*, 4629.

(9) Kotani, A.; Shin, S. *Rev. Mod. Phys.* **2001**, *73*, 203.

(10) The tolerance factor is defined as $t = (d_{A-O})/\sqrt{2}(d_{Mn-O})$, where A is the alkaline or alkali metal ion and O is the oxygen ion. This factor is a measure of the mismatch between equilibrium A−O and Mn−O bond lengths and the deviation of the Mn−O−Mn angle from 180°.

(11) Hwang, H. Y.; Cheong, S.-W.; Radaelli, P. G.; Marezio, M.; Batlogg, B. *Phys. Rev. Lett.* **1995**, *75*, 914.

(12) Malavasi, L.; Mozzati, M. C.; Ghigna, P.; Azzoni, C. B.; Flor, G. *J. Phys. Chem. B* **2003**, *107*, 2500. Malavasi, L.; Alessandri, I.; Mozzati, M. C.; Ghigna, P.; Chiodelli, G.; Azzoni, C. B.; Flor, G. *Phys. Chem. Chem. Phys.* **2003**, *5*, 2274.

(13) Vergara, J.; Ortega-Hertogs, R. J.; Madurga, V.; Sapiña, F.; El-Fadli, Z.; Martínez, E.; Beltrán, A.; Rao, K. V. *Phys. Rev. B* **1999**, *60*, 1127.

(14) Zangrando, M.; Finazzi, M.; Paolucci, G.; Comelli, G.; Diviacco, B.; Walker, R. P.; Cocco, D.; Parmigiani, F. *Rev Sci. Instrum.* **2001**, *72*, 1313.

(15) Zangrando, M.; Zacchigna, M.; Finazzi, M.; Cocco, D.; Rochow, R.; Parmigiani, F. *Rev Sci. Instrum.* **2004**, *75*, 31.

(16) Cocco, D.; Matteucci, M.; Prince, K.; Zangrando, M. *Proc. SPIE* **2001**, *4506*, 46.
(17) In-house UHV-modified back-illuminated 1340 × 1306 pixel^2 SX TE 1300/CCD made by Princeton Instruments.
(18) Mozzati, C. M.; Malavasi, L.; Ghigna, P.; Azzoni, C.; Flor, G. Unpublished results.
(19) Shimura, T.; Hayashi, T.; Inaguma, Y.; Itoh, M. *J. Solid State Chem.* **1996**, *124*, 250.
(20) Kurmaev, E. Z.; Korotin, M. A.; Galakhov, V. R.; Finkelstein, L. D.; Zabolotzky, E. I.; Efremova, N. N.; Stadler, S.; Ederer, D. L.; Moewes, A.; Bartkowski, S.; Neumann, M.; Matsuno, J.; Mizokawa, T.; Fujimori, A.; Mitchell, J. *J. Electron Spectrosc. Relat. Phenom.* **1999**, *103*, 793.
(21) Kurmaev, E. Z.; Cherkashenko, V. M.; Neumann, M.; Stadler, S.; Ederer, D. L.; Mukovskii, Y. M.; Solovyev, I. V.; Ovechkina, N. A.; Galakhov, V. R.; Fujimori, A.; Grush, M. M.; Callcott, T. A.; Perera, R. C. C. *J. Electron Spectrosc. Relat. Phenom.* **1998**, *96*, 187.
(22) Abbate, M.; DeGroot, F. M. F.; Fuggle, J. C.; Fujimori, A.; Strebel, O.; Lopez, F.; Domke, M.; Kaindl, G.; Sawatzky, G. A.; Takano, M.; Takeda, Y.; Eisaki, H.; Uchida, S. *Phys. Rev. B* **1992**, *46*, 4511.
(23) Ravindran, P.; Kjekshus, A.; Fjellvag, H.; Delin, A.; Eriksson, O. *Phys. Rev. B* **2002**, *65*, 064445.
(24) Sarma, D. D.; Shanthi, N.; Barman, S. R.; Hamada, N.; Sawada, H.; Terakura, K. *Phys. Rev. Lett.* **1995**, *75*, 1126.
(25) Okimoto, Y.; Katsufuji, T.; Ishikawa, T.; Arima, T.; Tokura, Y. *Phys. Rev. B* **1997**, *55*, 4206.
(26) Jung, J. H.; Kim, K. H.; Eom, D. J.; Noh, T. W.; Choi, E. J.; Yu, J. J.; Kwon, Y. S.; Chung, Y. *Phys. Rev. B* **1997**, *55*, 15489.
(27) Zhang, J.; McIlroy, D. N.; Dowben, P. A.; Liou, S. H.; Sabirianov, R. F.; Jaswal, S. S. *Solid State Commun.* **1996**, *97*, 39.
(28) Park, J.-H.; Kimura, T.; Tokura, Y. *Phys. Rev. B* **1998**, *58*, 13330.
(29) Park, J.-H.; Chen, C. T.; Cheong, S.-W.; Bao, W.; Meigs, G.; Chakarian, V.; Idzerda, Y. U. *Phys. Rev. Lett.* **1996**, *76*, 4215.
(30) Guo, J.-H.; Butorin, S. M.; Wassdahl, N.; Nordgren, J.; Berastegut, P.; Johansson, L.-G. *Phys. Rev. B* **2000**, *61*, 9140.
(31) Butorin, S. M.; Guo, J.-H.; Wassdahl, N.; Nordgren, J. *J. Electron Spectrosc. Relat. Phenom.* **2000**, *110*, 235.
(32) Kurmaev, E. Z.; Korotin, M. A.; Galakhov, V. R.; Finkelstein, L. D.; Zabolotzky, E. I.; Efremova, N. N.; Lobachevskaya, N. I.; Stadler, S.; Ederer, D. L.; Callcott, T. A.; Zhou, L.; Moewes, A.; Bartkowski, S.; Neumann, M.; Matsuno, J.; Mizokawa, T.; Fujimori, A.; Mitchell, J. *Phys. Rev. B* **1999**, *59*, 12799.